



Thermally activated flux flow in $\text{Fe}_{1.06}\text{Te}_{0.6}\text{Se}_{0.4}$ single crystal



M. Shahbazi^{a,*}, X.L. Wang^a, S.R. Ghorbani^{a,b}, S.X. Dou^a, C.T. Lin^c

^a Institute for Superconducting and Electronic Materials, Faculty of Engineering, Australian Institute for Innovative Materials, University of Wollongong, North Wollongong, NSW 2519, Australia

^b Department of Physics, Ferdowsi University of Mashhad, Mashhad, Iran

^c Max-Planck-Institut für Festkörperforschung, Heisenbergstr. 1, 70569 Stuttgart, Germany

ARTICLE INFO

Article history:

Received 2 June 2015

Revised 27 July 2015

Accepted 14 August 2015

Available online 7 September 2015

Keywords:

Iron based superconductors

Chalcogenides

Thermally activated flux flow

ABSTRACT

Resistivity of $\text{Fe}_{1.06}\text{Te}_{0.6}\text{Se}_{0.4}$ single crystal is investigated around superconducting transition region in different magnetic fields. The thermally activated energy (TAE) is analysed using the Arrhenius relation and modified thermally activated flux flow (TAFF) model. The results indicate that the Arrhenius curve slopes are directly related to but not equal to TAE. Therefore, use of the modified TAFF model is suggested, $\rho(T,B) = \rho_{0f} \exp(-U/T)$, where the temperature dependence of the pre-factor $\rho_{0f} = 2\rho_c U/T$ and the nonlinear relation of the TAE should be considered. The modified TAFF method results are in good agreement with the very high critical current density values from the experimental data. It was found that the vortex glass has a narrow region, and it depends weakly on magnetic field. The vortex phase diagram was determined based on the evolution of the vortex-glass transition temperature with magnetic field and the upper critical field.

Crown Copyright © 2015 Published by Elsevier B.V. All rights reserved.

1. Introduction

The capability to carry high transport current in magnetic field is one of the most significant aspects of superconductors. The limiting value of critical current is given by the balance between the pinning forces due to the spatial variation of condensation energy and, on the other hand, the Lorentz force applied by the transport current. Flux creep and flux flow are the two distinguishable regimes of dissipation. Flux creep occurs when the pinning force dominates and flux flow when the Lorentz force dominates. The activation energy for flux motion can be estimated from dc resistivity measurements. It is crucial to understand the thermally activated energy and the de-pinning critical current from both the practical and the fundamental points of view. Thermally activated energy (TAE) has been well studied in high temperature cuprates [1–5]. It is well known that the strong thermal fluctuation of high temperature superconductors is due to the very high transition temperature, short coherence length, and high anisotropy of these compounds, which result in broadening of the superconducting transition with applied magnetic field. Iron-based superconductors show a relatively high transition temperature, T_c , and short coherence length. They reveal nearly isotropic superconductivity, however, which makes them distinct from cuprates. For iron-based superconductors, the thermal fluctuations of vortices can lead

to thermally activated flux flow (TAFF), causing the resistance transition from the $R(T,B)$ curve to shift to lower temperatures and also broaden as the field increases. For example, $RE\text{FeAsO}_{1-x}\text{F}_x$ [6–10], where RE is a rare earth element, shows similar transition broadening to $\text{YBa}_2\text{Cu}_3\text{O}_{7-x}$ (YBCO) with increasing field. On the other hand, the thermal fluctuations are negligible in Ba-122 compounds, as the resistive transition curves $R(T,H)$ shift to lower temperature [11], but do not broaden as the field is increased. The broadening is intermediate for iron chalcogenides. $\text{FeSe}_{1-x}\text{Te}_x$ compounds have the tetragonal structure, where the Fe(Se/Te) layers are stacked along the c -axis, and have T_c as high as 15 K [12–14]. The antiferromagnetic order of FeTe is gradually suppressed by increasing x in $\text{FeTe}_{1-x}\text{Se}_x$, and the maximum T_c is achieved for $x = 0.5$ [13]. It was reported, however, that T_c can reach 37 K under pressure for FeSe compounds [15]. Possible superconductivity above 77 K in single unit cell FeSe films on SrTiO_3 (STO) substrate [16] has been reported very recently. The arsenic-free $\text{Fe}_{1+y}\text{Se}_{1-x}\text{Te}_x$ compounds are of great interest from the viewpoints of both the vortex state and practical applications. This is due to their simple structure and nearly isotropic upper critical field. Also, the high critical current density of $J_c > 10^6 \text{ A cm}^{-2}$ under the very high field of 30 T that has been recently achieved in $\text{FeSe}_{0.5}\text{Te}_{0.5}$ coated conductors [17] is another significant aspect of these compounds. In addition, as the iron is the only magnetic element in such compounds, it provides a unique opportunity to study the effects of excess iron in the Fe position on the vortex motion and thermally activated energy. Therefore, high quality single crystals of these compounds are the perfect candidates to study the vortex properties and thermally activated energy of the iron chalcogenides.

* Corresponding author. Tel.: +61 432 531 829.

E-mail address: msm979@uowmail.edu.au (M. Shahbazi).

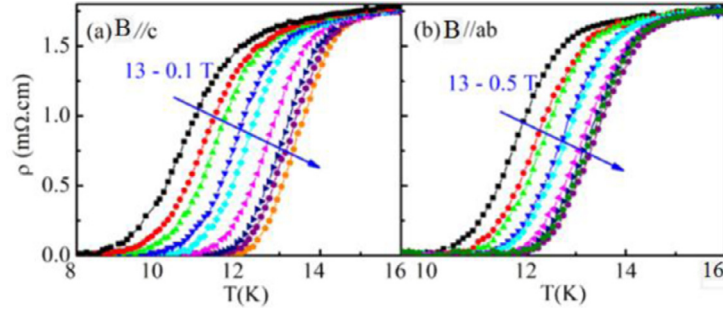


Fig. 1. Resistivity curves for $\text{Fe}_{1.06}\text{Te}_{0.6}\text{Se}_{0.4}$ single crystals under various applied magnetic fields for (a) $B//c$ and (b) $B//ab$.

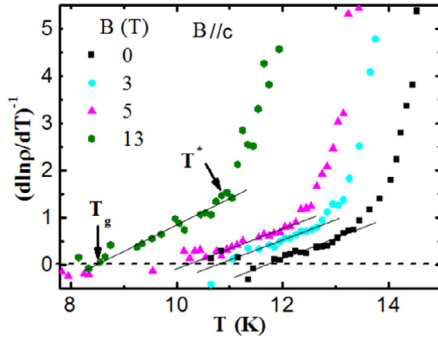


Fig. 2. Determination of the vortex glass transition temperature from Eq. (1) for $\text{Fe}_{1.06}\text{Te}_{0.6}\text{Se}_{0.4}$ at different magnetic fields.

In this paper, the thermally activated flux flow (TAFF) behaviour of $\text{Fe}_{1.06}\text{Te}_{0.6}\text{Se}_{0.4}$ single crystal is investigated in magnetic field up to 13 T, using the conventional Arrhenius relation and modified TAFF model. It will be shown that the Arrhenius curve slopes are directly related to, but not equal to, the activation energies of $\text{Fe}_{1.06}\text{Te}_{0.6}\text{Se}_{0.4}$ single crystal. Therefore, the use of a modified TAFF model, $\rho(T, B) = \rho_{0f} \exp(-U/T)$, is suggested, where the temperature dependence of the prefactor $\rho_{0f} = 2\rho_c U/T$ and the nonlinear relation of the thermal activation energy, $U(T, B)$, are considered. The modified TAFF method results are in good agreement with the very high J_c values from experimental data. It was found that $\text{Fe}_{1.06}\text{Te}_{0.6}\text{Se}_{0.4}$ superconductor can be regarded as both a 3D- and 2D-like system, which is dependent on the magnetic field direction in the TAFF region. The vortex phase diagram has been determined based on the evolution of the vortex-glass transition temperature, T_g , with magnetic field and the upper critical field.

2. Results and discussion

Fig. 1 shows the resistivity $\rho(T, B)$ of $\text{Fe}_{1.06}\text{Te}_{0.6}\text{Se}_{0.4}$ single crystal near T_c for $B//c$. The onset of T_c moves to lower temperature with increasing magnetic field.

According to the vortex phase transition theory [19], in the vortex glass state and close to the glass transition temperature, T_g , the resistivity disappears as a power law

$$\rho = \rho_0 |T/T_g - 1|^s \quad (1)$$

where s is a constant and depends on the kind of disorder, and ρ_0 is a characteristic resistivity that is related to the normal state. Therefore, the resistivity goes to zero at T_g . Consequently $T_g(B)$ can be extracted by applying the relation, $(d \ln \rho / dT)^{-1} \propto (T - T_g)/s$, to the resistive tails. Fig. 2 presents the resistivity of $\text{Fe}_{1.06}\text{Te}_{0.6}\text{Se}_{0.4}$ based on the vortex-glass model, Eq. (1), in the temperature range $T_g < T < T^*$, with intercept T_g and $s = 2.3 \pm 0.1$. It is clear that the resistivity can be well

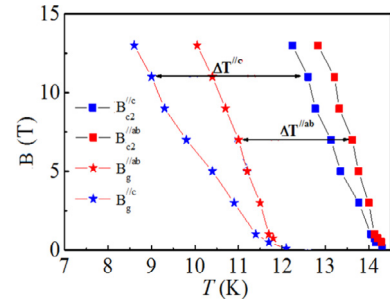


Fig. 3. Temperature dependence of B_{c2} for $B//ab$ and $B//c$. ΔT indicates the vortex-liquid region.

described by the vortex glass model. The estimated vortex glass transition line is shown in Fig. 2.

The upper critical field, B_{c2} , is characterized as the field at which the resistivity becomes 90% of the normal state resistivity. Fig. 3 shows B_{c2} as functions of temperature for $B//ab$ and $B//c$. B_{c2} exhibits a linear temperature dependence for both $B//ab$ and $B//c$. The estimated slopes for B_{c2} are -9.4 and -6.5 T/K for $B//ab$ and $B//c$, respectively. B_{c2} was estimated by using the conventional one-band Werthamer–Helfand–Hohenberg (WHH) theory: $B_{c2}(0) = -0.69T_c(dB_{c2}/dT)$, assuming that the upper critical field is limited by the orbital pair breaking effect. The estimated values of B_{c2} close to the zero temperature limit for $B//ab$ and $B//c$ are $\mu_0 B_{c2}^{ab} = 99.9$ T and $\mu_0 B_{c2}^c = 65$ T, respectively. The estimated B_{c2} calculated from the WHH theory is higher than the Bardeen Cooper Schrieffer (BCS) paramagnetic limit, B_p^{BCS} , in the weak coupling regime. By using the weak coupling BCS formula, $B_p^{BCS} = 1.84T_c$, we obtain $B_p^{BCS} = 28.3$ T and 26.7 T for $B//ab$ and $B//c$, respectively. The estimated B_{c2}^{ab} and B_{c2}^c from the WHH formula are 3.5 and 2.4 times the limits for $B//ab$ and $B//c$, respectively, indicating that Zeeman paramagnetic pair breaking possibly is essential for both directions. Also, it reveals the unconventional superconducting mechanism in this family. The anisotropy value, Γ , obtained using $\Gamma = B_{c2}^{ab}/B_{c2}^c$, is equal to 1.5. According to the collective pinning model [20], the disorder-induced spatial fluctuations in the solid-vortex lattice can be clearly divided into markedly different regimes according to the strength of the applied field. Two different regimes are distinguishable: (1) the vortex glass, which governs the region below the transition field, B_g ; and (2) the vortex liquid, which holds between B_g and B_{c2} , where thermal fluctuations are important. As can be seen from Fig. 3, the vortex-glass phase indicates that the $\text{Fe}_{1.06}\text{Te}_{0.6}\text{Se}_{0.4}$ single crystal features only a narrow region of the vortex-liquid phase, which is denoted by ΔT , with a $\Delta T^c/c$ and $\Delta T^{ab/ab}$ of 3.1 ± 0.5 K and 2.6 ± 0.2 K, respectively, at magnetic field of 0 up to 13 T. This result suggests that the vortex-glass region depends weakly on magnetic field, which originates from the vastly enhanced vortex pinning in the studied magnetic field levels.

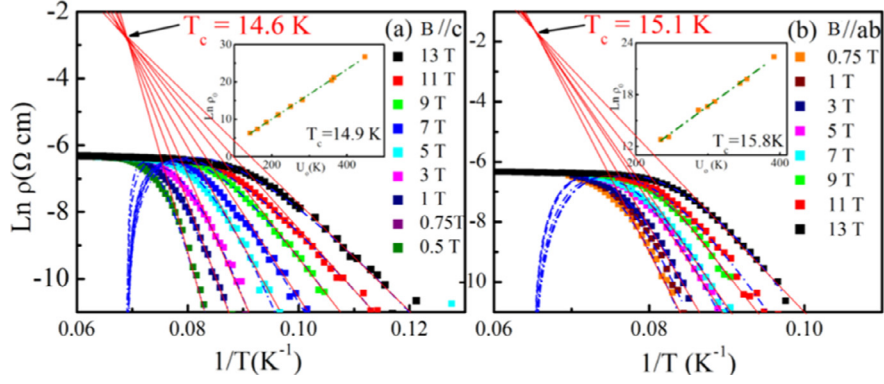


Fig. 4. Longitudinal resistivity in different magnetic fields for (a) $B//c$ and (b) $B//ab$. The corresponding solid red lines and blue dashed lines are fitting results from the Arrhenius relation and Eq. (6), respectively. The insets show $\text{Ln } \rho_0$ vs. U_0 data, which were obtained by using Arrhenius plots. The green dashed line is the linear fit to the inferred data. (For interpretation of the references to colour in this figure legend, the reader is referred to the web version of this article.)

Based on the TAFF theory [2,20], the resistivity in the TAFF regime can be written as:

$$\rho = \left(\frac{2\nu_0 LB}{J} \right) \exp\left(-\frac{Jc_0 BVL}{T}\right) \sinh\left(\frac{J BVL}{T}\right) \quad (3)$$

where ν_0 is the attempt frequency for a flux bundle of volume V , L is the hopping distance, B is the magnetic induction, J is the applied current density, Jc_0 is the critical current density in the absence of flux creep, and T is the temperature. If $J BVL \ll 1T$, $B) = (2\rho_c U/T) \exp(-U/T) = \rho_{of} \exp(-U/T)$ and J is small enough, then Eq. (3) can be rewritten as:

$$\rho(T, B) = (2\rho_c U/T) \exp(-U/T) = \rho_{of} \exp(-U/T) \quad (4)$$

Here $U = Jc_0 BVL$ is the thermal activation energy (TAE), $\rho_c = \nu LB/Jc_0$, and $\rho_c U/T$ is considered as the prefactor ρ_{of} . Mostly, the TAE of cuprates and iron-based superconductors (FBSS) is analysed using Eq. (4), assuming that the $2\rho_c U/T$ is temperature independent. Then $U(T, B) = U_0(B) (1 - t)$, where $t = T/T_c$, and $\text{Ln } \rho$ vs. $1/T$ becomes the Arrhenius relation, $\text{Ln } \rho(T, B) = \text{Ln } \rho_0(B) - U_0(B)/T$. Here, B is the magnetic field strength, and $\text{Ln } \rho_0(B) = \text{Ln } \rho_{of} + U_0(B)/T_c$. Moreover, it can be resolved that $\partial \text{Ln } \rho / \partial (1/T) = U_0(B)$. Therefore, $\text{Ln } \rho$ vs. $1/T$ should be linear in the TAFF regime where the slope is $U_0(B)$, and its y intercept is represented by $\text{Ln } \rho_0(B)$. It is likely that $U \neq U_0 (1 - t)$ and $\rho_{of} \neq$ are constant; however, as the lowest temperature part of the $\rho(T)$ curve is used for determination of U_0 in the Arrhenius model. It is suggested [3] that the temperature dependence of ρ_{of} in Eq. (4) should be taken into account in the analysis. According to the condensation model, $U_0 \propto B_c^2(t) \xi^n(t)$, where H_c is the thermodynamic critical field, ξ is the coherence length, $t = T/T_c$, and $0 < n < 3^1$, depending on the dimensionality of the vortex system. Since $B_c(t) \propto 1 - t$ and $\xi(t) \propto (1 - t)^{-1/2}$ near T_c then

$$U(T, B) = U_0(B) (1 - t)^q \quad (5)$$

Generally, $q = 1.5$ is observed in high temperature superconductors showing 3D behaviour, whereas $q = 2$ represents 2D behaviour [21–23]. Combining Eqs. (4) and (5), it can be derived that

$$\text{Ln } \rho = \text{Ln}(2\rho_c U_0) + q \text{Ln}(1 - t) - \text{Ln } T - U_0(1 - t)^q / T \quad (6)$$

where ρ_c and U_0 are temperature independent and T_c is obtained from the Arrhenius fitting. Therefore, the slope of the Arrhenius plot near T_c is given by:

$$\frac{\partial \text{Ln } \rho}{\partial (1/T)} = [U_0(1 - t)^q - T] \left[1 + \frac{qt}{1 - t} \right] \quad (7)$$

Eq. (7) is known as the modified TAFF model, and the fit using this model is in better agreement with experimental results than the Arrhenius model for cuprates and some iron-based superconductors [2,3,9,24,25]. According to Eq. (7), the activation energy obtained

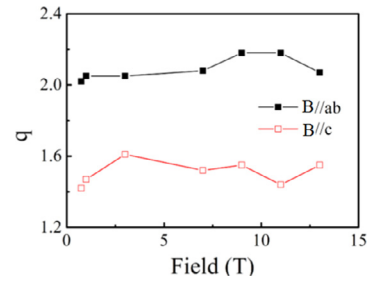


Fig. 5. q as a function of magnetic field. It is obtained from fitting the resistivity in the TAFF regime using Eq. (6) for both $B//ab$ and $B//c$.

from the slope of the Arrhenius plot near T_c is increased with respect to the actual value by $[1 + qt / (1 - t)]$. As the U_0 is strongly temperature dependent near T_c , the enhancement is large.

Fig. 4 presents the Arrhenius plots of $\rho(1/T)$ at different magnetic fields for $B//ab$ and $B//c$. The red solid lines show the results of linear fitting in the low-resistivity range. All the linear fittings cross at approximately T_c , which is about 14.6 and 15.1 K for $B//c$ and $B//ab$, respectively. The slope of these Arrhenius plots for low resistivity can be related to the activation energy. The insets show $\text{Ln } \rho_0$ vs. U_0 , which are obtained from the linear fits of the Arrhenius results. Based on $\text{Ln } \rho_0(B) = \text{Ln } \rho_{of} + U_0(B)/T_c$, $\text{Ln } \rho_{of}$ and T_c can be obtained by linear fitting.

The values of $T_c = 14.9$ and 15.8 K for $B//c$ and $B//ab$, respectively, are in good agreement with the obtained values of T_{cross} , the points where the linear fits cross, within the range of error. It is likely that the obtained values of U_0 are not accurate enough, as they are only estimated based on the lowest temperature part of the $\rho(T)$ curve in a very narrow area, i.e., the Arrhenius relation in the TAFF region. Then, the effects of the nonlinear relationship of $U(T, B)$ against T and the temperature dependence of ρ_c should be considered. Therefore, Eq. (6) was fitted to the experimental data. The blue dashed curves in Fig. 4 represent the results from Eq. (6). All fits are in good agreement with the experimental data, and the results are more accurate than the Arrhenius model, which just covers a very narrow resistivity area at low temperature.

It should be emphasized that the actual value of U_0 is two times higher for $B//ab$ than in the $B//c$ direction. It is likely that the coupling strength between the FeSe planes, which determines the pinning behaviour, is more effective than the actual defect structure [1].

Fig. 5 presents the magnetic field dependence of q , which is obtained from the best fits of the experimental data to Eq. (6) for $B//ab$ and $B//c$. The value of q is 2.1 ± 0.1 for $B//ab$. For $B//c$, the value of q in $\text{Fe}_{1.06}\text{Te}_{0.6}\text{Se}_{0.4}$ single crystals is about 1.5 ± 0.1 , which is similar

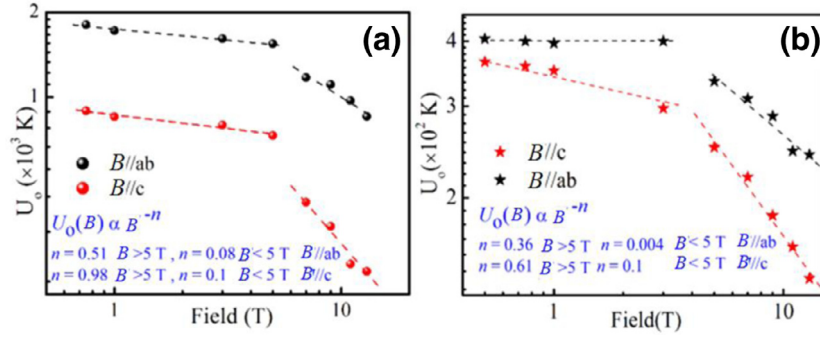


Fig. 6. Magnetic field dependence of U_0 obtained from (a) the modified TAFF model (Eq. (3)) and (b) the Arrhenius relationship for $B//ab$ and $B//c$. The dashed lines are power law fittings using $U_0(B) \propto B^{-n}$.

to estimated $q = 1.5$ in LiFeAs crystal [20], but is different from the value of $q = 2$ in $\text{Fe}_{1+y}(\text{Te}_{1-x}\text{S}_x)_z$ [19], $\text{SmFeAs}_{0.9}\text{F}_{0.1}$ [9], and many cuprates [3,5], which generally show 2-dimensional behaviour with a similar scaling. Therefore, $\text{Fe}_{1.06}\text{Te}_{0.6}\text{Se}_{0.4}$ superconductor has a small anisotropy like that of LiFeAs superconductor and can be regarded as a 3D-like system in the TAFF region for $B//c$. The different values of q for $B//c$ and $B//ab$ indicate that the dimensionality for $B//ab$ is very much closer to two-dimensional behaviour than that for $B//c$. These results suggest that the temperature dependence of the pinning potential is correlated with dimensionality behaviour in $\text{Fe}_{1.06}\text{Te}_{0.6}\text{Se}_{0.4}$ single crystal. Therefore, one can tune the effective pinning potential with the direction of the applied magnetic field with respect to the c -axis or ab -plane directions, and the crossover from 2D to 3D can be found.

Fig. 6 shows the magnetic field dependence of U_0 obtained from (a) the modified TAFF model using Eq. (5) and (b) the Arrhenius relationship for $B//ab$ and $B//c$. In both field directions, $U_0(B)$ indicates power law field dependence for both the modified TAFF model and the Arrhenius relation. Using the modified TAFF model, for $B//ab$, $n = 0.51$ for $B > 5$ T and $n = 0.08$ for $B < 5$ T, while for $B//c$, $n = 0.98$ for $B > 5$ T and $n = 0.1$ for $B < 5$ T. It is likely that single vortex pinning is dominant at low magnetic field, as U_0 decreases very slowly with increasing magnetic field [21]. On the other hand, U_0 becomes strongly field dependent for $B > 5$ T, indicating the crossover from single vortex pinning to a collective pinning regime, as the vortex spacing becomes significantly smaller than the penetration depth in higher fields. The obtained values of U_0 using the Arrhenius relation are nearly five times smaller than the obtained values using the modified TAFF model at low magnetic field. The higher value of U_0 obtained from the modified TAFF model is in good agreement with the high value of the critical current density due to the high pinning potential in this compound [22,17]. The trend in $U_0(B)$ is similar in both models, however. In other words, $U_0(B)$ is revealed to be weakly field

dependent for $B < 5$ T, but it becomes strongly field dependent for $B > 5$ T. It is likely that the slopes of the Arrhenius plots are directly related to, but not equal to, the real value of the activation energy. Similar behaviour has been reported for $\text{YBa}_2\text{Cu}_3\text{O}_7$ single crystals [1].

The values of U_0 are estimated from the limited temperature interval where the data reveal linear behaviour on the Arrhenius plot. Even if the slope does not change significantly in this temperature interval, it does not demonstrate that U_0 is temperature independent or not, $-\text{d}(\ln \rho)/\text{d}(1/T)$ was plotted as a function of temperature in different magnetic fields for $B//ab$ and $B//c$ in Fig. 7. In the normal state for $T > T_c$, $-\text{d}(\ln \rho)/\text{d}(1/T)$ is almost temperature and magnetic field independent, but then for $T < T_c$, it gradually increases with the onset of superconductivity. Then, it is enhanced sharply in the superconducting regime with increasing temperature, which is related to the TAFF regime. If $U(T,B) = U_0(B)(1-t)$ and $\rho_{\text{of}} = \text{const}$, then $-\text{d}(\ln \rho)/\text{d}(1/T) = U_0(B)$, and therefore, $U_0(B)$ should be a set of horizontal lines. The horizontal red lines in Fig. 7 represent the $U_0(B)$ values, with each of them having a limited length. Each length covers the temperature interval that relates to the interval of $1/T$ for estimating $U_0(B)$ in the Arrhenius plot. It should be noted that the slopes change with temperature without reaching a constant value. The $-\text{d}(\ln \rho)/\text{d}(1/T)$ curve increases with decreasing temperature and almost crosses the centre of the horizontal $U_0(B)$ lines. This means that $U(T,B) \neq U_0(B)(1-t)$ and ρ_{of} is temperature dependent, while each $U_0(B)$ value is only the average value of $-\text{d}(\ln \rho)/\text{d}(1/T)$ in the temperature area of the fitting, and the values of U_0 obtained from the Arrhenius relation are estimated in a very narrow temperature interval. Therefore, it is likely that the $U_0(B)$ values estimated from the conventional Arrhenius model are not accurate enough. Then, the temperature dependence of ρ_{of} and the nonlinear relation of $U(T,B)$ should be considered [3]. The dashed green lines in Fig. 7 are

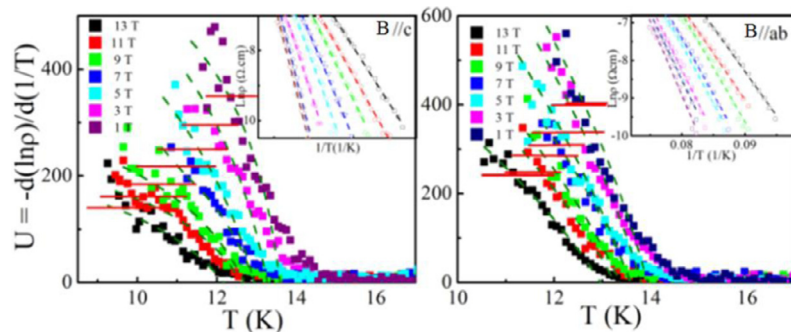


Fig. 7. $-\text{d}(\ln \rho)/\text{d}(1/T)$ as a function of temperature in different magnetic fields for $B//c$ and $B//ab$. The solid red lines represents the U_0 obtained from linear fitting of the Arrhenius relation, and the green dashed curves are plotted using Eq. (6), with the fitting parameters $U_0(B)$ and q obtained from the modified TAFF model (Eq. (5) in Fig. 5). The insets show the inverse temperature dependence of $\ln \rho$. (For interpretation of the references to colour in this figure legend, the reader is referred to the web version of this article.)

plotted using Eq. (7). The U_0 and q parameters were determined by fitting Eq. (5) to the corresponding resistivity data in Fig. 4. It is obvious that the modified TAFF model can effectively fit the upturn trend of $-(\ln \rho)/d(1/T)$ with decreasing temperature and can give a more accurate value of $U_0(B)$ compared to the Arrhenius relation.

In summary, it is shown that the Arrhenius curve slopes are directly related to, but not equal to, the activation energies in $\text{Fe}_{1.06}\text{Te}_{0.6}\text{Se}_{0.4}$ single crystals. Therefore, use of the modified TAFF model is suggested, where the temperature dependence of ρ_{0f} and the nonlinear relation of $U(T,B)$ should be considered. The modified TAFF method results are closer to the experimental data. It was found that there is a correlation between the effective pinning potential, the temperature, and the magnetic field, which is governed by the dimensionality of the $\text{Fe}_{1.06}\text{Te}_{0.6}\text{Se}_{0.4}$ crystal.

3. Methods

Single crystals of $\text{Fe}_{1.06}\text{Te}_{0.6}\text{Se}_{0.4}$ were prepared by a self-flux method. Details of the single crystal growth are reported elsewhere [18]. The as-grown single crystal was cleaved and cut into a rectangular shape with the size of $1.46 \times 2.12 \times 0.06 \text{ mm}^3$ for transport and magnetic measurements. The transport properties were measured over a wide range of temperatures and magnetic fields up to 13 T, with applied current of 5 mA, using a physical properties measurement system (PPMS, Quantum Design).

Acknowledgment

This work was supported by the Australian Research Council (ARC) through Discovery Project DP 1094073. M Shahbazi would like thank Australian Institute of Nuclear Science and Engineering (AINSE) for their support.

Author contributions: M.S. designed and performed all the magnetic and transport measurements and collected the data. C.T. Lin provided samples for this work. M.S., X.L.W., R.G. and S.X.D. contributed to the discussions and analysis of the data. M.S., X.L.W., and R.G. co-wrote the paper.

References

- [1] T. Palstra, B. Batlogg, R. van Dover, L. Schneemeyer, J. Waszczak, Dissipative flux motion in high-temperature superconductors, *Phys. Rev. B* 41 (1990) 6621.
- [2] T. Palstra, B. Batlogg, L. Schneemeyer, J. Waszczak, Thermally activated dissipation in $\text{Bi}_{2.2}\text{Sr}_2\text{Ca}_{0.8}\text{Cu}_2\text{O}_{8+\delta}$, *Phys. Rev. Lett.* 61 (1988) 1662.
- [3] Y. Zhang, H. Wen, Z. Wang, Thermally activated energies of $\text{YBa}_2\text{Cu}_3\text{O}_{7-\delta}$ and $\text{Y}_{0.8}\text{Ca}_{0.2}\text{Ba}_2\text{Cu}_3\text{O}_{7-\delta}$ thin films, *Phys. Rev. B* 74 (2006) 144521.
- [4] D. Kim, K. Gray, R. Kampwirth, D. McKay, Possible origins of resistive tails and critical currents in high-temperature superconductors in a magnetic field, *Phys. Rev. B* 42 (1990) 6249.
- [5] Y. Zhang, Z. Wang, X. Lu, H. Wen, J. de Marneffe, R. Deltour, A. Jansen, P. Wyder, Deviations from plastic barriers in $\text{Bi}_2\text{Sr}_2\text{CaCu}_2\text{O}_{8+\delta}$ thin films, *Phys. Rev. B* 71 (2005) 052502.
- [6] J. Jaroszynski, F. Hunte, L. Balicas, Youn-jung Jo, I. Raičević, A. Gurevich, D. Larbalestier, F. Balakirev, L. Fang, P. Cheng, Y. Jia, H. Wen, Upper critical fields and thermally-activated transport of $\text{NdFeAsO}_{0.7}\text{F}_{0.3}$ single crystal, *Phys. Rev. B* 78 (2008) 174523.
- [7] M. Shahbazi, X.L. Wang, C. Shekhar, O.N. Srivastava, S.X. Dou, Upper critical field, critical current density and thermally activated flux flow in fluorine doped Ce-FeAsO superconductors, *Supercond. Sci. Technol.* 23 (2010) 105008.
- [8] M. Shahbazi, X.L. Wang, C. Shekhar, O.N. Srivastava, Z.W. Lin, J.G. Zhu, S.X. Dou, Upper critical field and thermally activated flux flow in $\text{LaFeAsO}_{1-x}\text{F}_x$, *J. Appl. Phys.* 109 (2011) 07E162.
- [9] Y.Z. Zhang, Z.A. Ren, Z.X. Zhao, Thermally activated energy and critical magnetic fields of $\text{SmFeAsO}_{0.9}\text{F}_{0.1}$, *Supercond. Sci. Technol.* 22 (2009) 065012.
- [10] Xiaolin Wang, Shaban Reza Ghorbani, Germanas Peleckis, Shixue Dou, Very high critical field and superior J_c -field performance in $\text{NdFeAsO}_{0.82}\text{F}_{0.18}$ with T_c of 51 K, *Adv. Mater.* 21 (2009) 236.
- [11] Xiao-Lin Wang, S.R. Ghorbani, Sung-Ik Lee, S.X. Dou, C.T. Lin, T.H. Johansen, K.H. Müller, Z.X. Cheng, G. Peleckis, M. Shahbazi, A.J. Quiviller, V.V. Yurchenko, G.L. Sun, D.L. Sun, Very strong intrinsic flux pinning and vortex avalanches in $(\text{Ba,K})\text{Fe}_2\text{As}_2$ superconducting single crystals, *Phys. Rev. B* 82 (2010) 024525.
- [12] K.W. Yeh, C.T. Ke, T.W. Huang, T.K. Chen, Y.L. Huang, P.M. Wu, M.K. Wu, Superconducting $\text{FeSe}_{1-x}\text{Te}_x$ single crystals grown by optical zone-melting technique, *Cryst. Growth Des.* 9 (2009) 4847.
- [13] M.H. Fang, H.M. Pham, B. Qian, T.J. Liu, E.K. Vehstedt, Y. Liu, L. Spinu, Z.Q. Mao, Superconductivity close to magnetic instability in $\text{Fe}(\text{Se}_{1-x}\text{Te}_x)_{0.82}$, *Phys. Rev. B* 78 (2008) 224503.
- [14] B.C. Sales, A.S. Sefat, M.A. McGuire, R.Y. Jin, D. Mandrus, Y. Mozharivskiy, Bulk superconductivity at 14 K in single crystals of $\text{Fe}_{1+y}\text{Te}_x\text{Se}_{1-x}$, *Phys. Rev. B* 79 (2009) 094521.
- [15] S. Margadonna, Y. Takabayashi, Y. Ohishi, Y. Mizuguchi, Y. Takano, T. Kagayama, T. Nakagawa, M. Takata, K. Prassides, Pressure evolution of the low-temperature crystal structure and bonding of the superconductor FeSe ($T_c=37$ K), *Phys. Rev. B* 80 (2009) 064506.
- [16] Qing-Yan Wang, Zhi Li, Wen-Hao Zhang, Zuo-Cheng Zhang, Jin-Song Zhang, Wei Li, Hao Ding, Yun-Bo Ou, Peng Deng, Kai Chang, Jing Wen, Can-Li Song, Ke He, Jin-Feng Jia, Shuai-Hua Ji, Ya-Yu Wang, Li-Li Wang, Xi Chen, Xu-Cun Ma, Qi-Kun Xue, Interface-induced high-temperature superconductivity in single unit-cell FeSe films on SrTiO_3 , *Chin. Phys. Lett.* 29 (2012) 037402.
- [17] W. Si, S.J. Han, X. Shi, S.N. Ehrlich, J. Jaroszynski, A. Goyal, Q. Li, High current superconductivity in $\text{FeSe}_{0.5}\text{Te}_{0.5}$ coated conductors at 30 Tesla, *Nat. Commun.* 4 (2013) 1347.
- [18] Y. Liu, C.T. Lin, A comparative study of $\text{Fe}_{1+\delta}\text{Te}_{1-x}\text{Se}_x$ single crystals grown by Bridgman and self-flux techniques, *J. Supercond. Nov. Magn.* 24 (2011) 183.
- [19] Daniel S. Fisher, Matthew P.A. Fisher, David A. Huse, Thermal fluctuations, quenched disorder, phase transitions, and transport in type-II superconductors, *Phys. Rev. B* 43 (1991) 130.
- [20] G. Blatter, V.B. Geshkenbein, A.I. Larkin, V.M. Vinokur, Vortices in high-temperature superconductors, *Rev. Mod. Phys.* 66 (1994) 1125.
- [21] M. Tinkham, Resistive transition of high-temperature superconductors, *Phys. Rev. Lett.* 61 (1988) 1658.
- [22] Y. Yeshurun, A. Malozemoff, Giant flux creep and irreversibility in an Y-Ba-Cu-O crystal: an alternative to the superconducting-glass model, *Phys. Rev. Lett.* 60 (1988) 2202.
- [23] Z.H. Wang, X.W. Cao, The effective activation energy $U_e(T,H)$ in epitaxial $\text{GdBa}_2\text{Cu}_3\text{O}_7$ - thin film, *Solid State Commun.* 109 (1999) 709.
- [24] Hechang Lei, Rongwei Hu, E.S. Choi, C. Petrovic, Thermally activated energy and flux-flow Hall effect of $\text{Fe}_{1+y}(\text{Te}_{1-x}\text{S}_x)_z$, *Phys. Rev. B* 82 (2010) 134525.
- [25] Song Jang, Kang Yoo, Rhee Byeongwon, Jong-Soo, Yong Seung Kwon, Thermally activated flux flow and fluctuation conductivity in LiFeAs single crystal, *Europhys. Lett.* 97 (2012) 47003.